Three-dimensional imaging of human brain tissues using absorption-contrast high-resolution X-ray tomography

Anna Khimchenko[a*], Georg Schulz[a], Christos Bikis[a], Hans Deyhle[a], Natalia Chicherova[a, b], Simone E. Hieber[a], Gabriel Schweighauser[c], Jürgen Hench[c], and Bert Müller[a]

[a] Biomaterials Science Center, Department of Biomedical Engineering, University of Basel, Gewerbestrasse 14, 4123 Allschwil, Switzerland;
[b] Medical Image Analysis Center, Department of Biomedical Engineering, University of Basel, Gewerbestrasse 14, 4123 Allschwil, Switzerland;
[c] Institute of Pathology, Department of Neuropathology, Basel University Hospital, Schönbeinstrasse 40, 4056 Basel, Switzerland

ABSTRACT

Our body is hierarchically organized down to individual cells. Cutting-edge clinical imaging facilities reach a spatial resolution of a fraction of a millimeter, living cells invisible. A decade ago, post-mortem X-ray imaging by means of synchrotron radiation enabled the identification of Os-stained ganglion and unstained Purkinje cells. Very recently, even sub-cellular structures, such as nucleolus and the dendritic tree of Purkinje cells, were extracted by means of phase-contrast single-distance synchrotron radiation-based hard X-ray tomography. At the same time, conventional absorption-contrast, laboratory-based micro computed tomography was successfully applied to visualize brain components including individual Purkinje cells within a cerebellum specimen. Thus, the goal of isotropic-cellular-resolution visualization of soft tissues within a laboratory environment without application of any dedicated contrast agent was achieved. In this communication, we are discussing (1) to which extend the quality gain of the laboratory-based absorption-contrast tomography can be driven with respect to optical microscopy of stained tissue sections and (2) what value such a technique would add. As a proof of principle, four histological sections were affine-registered to corresponding three-dimensional (3D) tomography dataset. We are discussing a semi-automatic landmark-based 2D-3D registration framework and compare registration results based on mean square difference (MSD) metrics.

Keywords: X-ray micro computed tomography, absorption-contrast, brain tissue, cerebellum, laboratory-based tomography, Purkinje cell, 2D-3D registration.

1. INTRODUCTION

Biologically inspired designs and principles can be found in a broad range of technical applications. The complexity of biological structures makes it highly challenging to engineer and manufacture bio-inspired components, as they frequently have a hierarchical multi-scale structural organization which contains randomly organized parts. These are, nevertheless, essential for proper function. There is a direct correlation between performed functions and structural organization. Visualization is highly relevant to bio-replication, as can help in uncovering structural organization down to the a microscopic level.

The brain is one of the most complex[1] and important organs of the human body.[2] It contains billions of neurons which significantly vary in shape and size, see Figure 1. Similarly diverse are diseases affecting this vital organ. Thus, studying brain micro-morphology is of high interest. The most common method to study soft tissue morphology on a cellular level within a laboratory environment, optical microscopy of stained tissue sections, typically remains limited to two-dimensional (2D) investigation. Histological serial sectioning is time-consuming and prone to artifacts, such as deformation or rupture, making it laborious to reconstruct a three-dimensional (3D) volume from individual sections.[3]

* anna.khimchenko@unibas.ch; phone: +41 61 207 54 41; fax: +41 61 207 54 99; bmc.unibas.ch

Bioinspiration, Biomimetics, and Bioreplication 2017, edited by Mato Knez, Akhlesh Lakhtakia, Raúl J. Martín-Palma
Proc. of SPIE Vol. 10162, 101620K · © 2017 SPIE · CCC code: 0277-786X/17/$18 · doi: 10.1117/12.2259977

Visualization of volumes has considerable advantages over visualization of individual sections.[4] *In vivo* modalities established in daily clinical practice, such as magnetic resonance imaging (MRI), do not provide cellular resolution. Serial sectioning imaging[5–7] can reach cellular resolution in 3D; however, requires a complex volume reconstruction,[3] are destructive and does not provide isotropic resolution. Sectioning-free methods combined with clearing or tissue-transformation[8,9] to increase penetration depth have successfully been developed, however, they remain limited in terms of maximum sample sizes in the millimetre-range.[4] Thus, the possibility to perform high-sensitivity and -resolution imaging of relatively large tissue volumes in a non-destructive and time-efficient manner within the laboratory environment is of high interest.

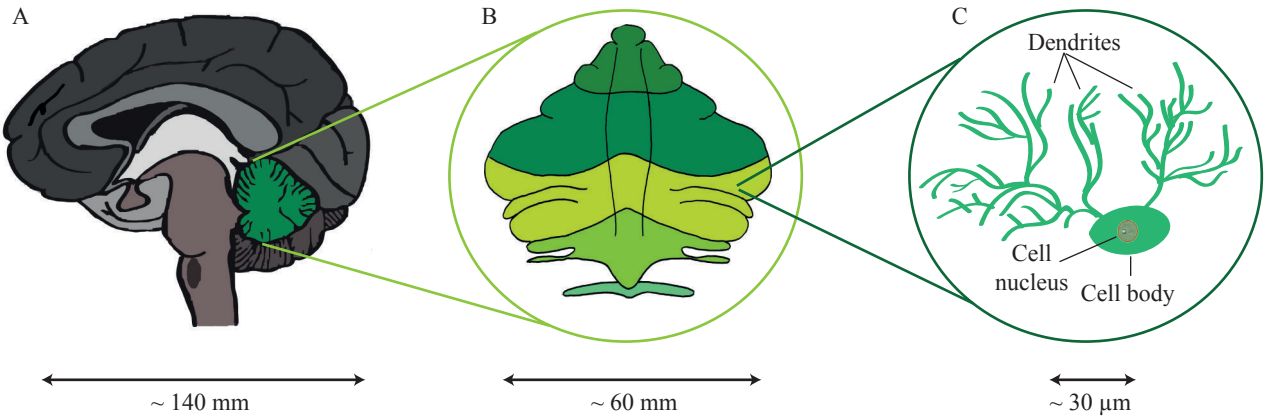

Figure 1. Schematic representation of the hierarchical multi-scale organization of human brain. A: complete brain, B: cerebellum, C: individual neuron with sub-cellular anatomical structures.

A decade ago, *post-mortem* X-ray imaging by means of synchrotron radiation enabled the identification of Os-stained ganglion[10] and non-stained Purkinje cells.[11] Very recently, even sub-cellular structures, which comprise the nucleolus and the dendritic tree of the Purkinje cells, were extracted and automatically quantified by means of single-distance phase-contrast synchrotron radiation-based hard X-ray tomography.[12] Also recently, conventional absorption-contrast laboratory-based micro computed tomography (µCT) was successfully applied to visualize brain components including individual Purkinje cells.[13]

Micro computed tomography is a 3D imaging modality that yields true micrometer resolution in a non-destructive and time-efficient manner. Thus, µCT enables the 3D visualization and quantification of tissues prior to histological sectioning[11,14] providing a valuable complement and enabling the possibility of virtual histology. In this communication, the tomography data derived from a formalin-fixed paraffin-embedded (FFPE) human cerebellum block are compared to hematoxylin and eosin (H&E) stained histological sections. For this purpose, four histological sections were elastically registered in the three-dimensional tomography dataset. We are discussing some of the possible semi-automatic landmark-based frameworks for registration of tomography and histology, and compare registration results based on the mean square difference (MSD) metrics. We demonstrate potential benefits of hard X-ray micro computed tomography for the investigation of soft tissues. In addition, we are discussing how far the quality gain of the laboratory-based absorption-contrast can be driven with respect to the optical microscopy of stained tissue sections and its benefits compared to microscopy alone.

Our society is ageing and neurodegenerative diseases have become a severe problem that will worsen with time as their incidences increase with age. These diseases dramatically affect the daily life of the respective subject and their families. Although neurodegenerative deceases frequently present with diverse clinical symptoms, the majority of them are characterized on the basis of intracellular changes. The possibility to visualize relatively large tissue volumes down to cellular level is highly beneficial to study tissues in health and disease.

2. MATERIALS AND METHODS

2.1 Specimen preparation

The human cerebellum block was extracted from a donated cadaveric body of a 73-year-old male and visualized *post mortem*. Written consent for scientific use was documented and all procedures were conducted in accordance with the Declaration of Helsinki. Routine sample preparation and paraffin-embedding protocols were applied and carried out in a diagnostic neuropathology laboratory without any modifications, for more details see.[12,13] After paraffin embedding a cylinder 6 mm in diameter was extracted using a metal punch.

2.2 Laboratory-based absorption-contrast µCT

Laboratory-based µCT experiment was carried out using the µCT system nanotom® m (phoenix|x-ray, GE Sensing & Inspection Technologies GmbH, Wunstorf, Germany), see Figure 2. The system is equipped with a 180 kV - 15 W nano-focus® tube with tungsten (W) transmission target[15,16] and a temperature stabilized digital GE DXR 500L detector. The µCT was performed with an effective pixel size of 3.5 µm, acceleration voltage 60 kVp, tube current 350 µA and exposure time 3 s per projection. For the acquisition, 1900 angular projections were recorded. The measurement was taken in the tube operation mode "0" with an estimated source size of 2.7 µm, as specified by the supplier. Data acquisition and reconstruction were performed automatically with the datos|x 2.0 software (phoenix|x-ray, GE Sensing & Inspection Technologies GmbH, Wunstorf, Germany). The total acquisition time is less then 2 hours and reconstruction was performed within minutes.

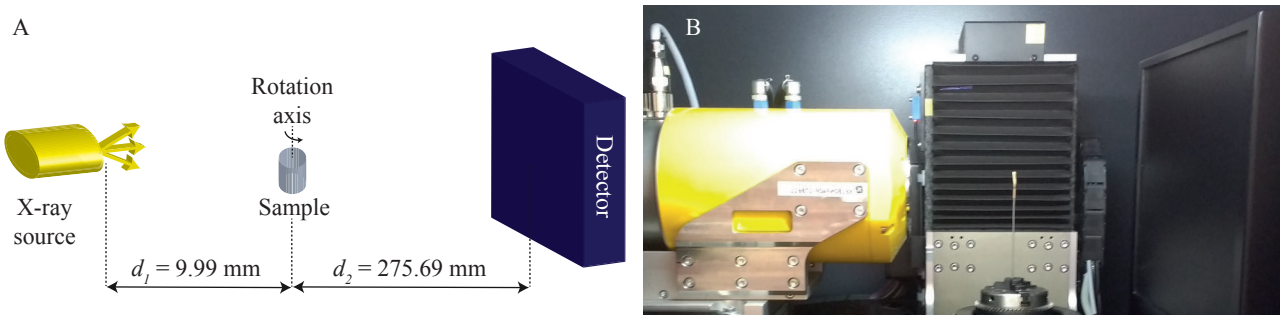

Figure 2. (A) Scheme and (B) photograph of the laboratory-based absorption-contrast micro computed tomography set-up. For measurement, the sample was mounted on a precision rotation stage and positioned between the X-ray source and detector. d_1: focus object distance (FOD), d_2: object detector distance (ODD).

2.3 Histology

Subsequent to the laboratory-based µCT measurement, the specimen was investigated by means of histology after re-embedded. Sections of 4 µm thickness were cut using a microtome, mounted on glass slides, and stained with hematoxylin and eosin (H&E) based on standard histological protocols. Images of the resulting slides were taken on a light microscope and resulted in isotropic pixel sizes of 6.99 µm, for more details see.[12,13]

2.4 Data registration

A semi-automatic landmark-based 2D-3D registration of four histological sections within the tomographic dataset was performed.[17] The first step is the manual identification of feature points between histological sections and µCT volume.[18] For this purpose, characteristic vessels, cell groups and cracks seen in both datasets were matched. The 3D coordinates of the matching points in the µCT data were stored. A surface was fitted to the landmarks based on several models using the Curve Fitting Toolbox™ implemented in Matlab R2014a. In total, eight surface fitting models were used: quadratic polynomial surface (poly22), polynomial surface with degree two in one axis and three in other (poly23), cubic polynomial surface (poly33), polynomial surface with degree four (poly44), polynomial surface with degree five (poly55), polynomial surface based on piecewise cubic interpolation (spline), polynomial surface based on local linear regression (linear), polynomial surface based on thin plate model (plate). These surfaces were considered to correspond to the location of the histological sections in the volume. The corresponding registered tomography slices were interpolated from the µCT volume using

the obtained coordinates of the surfaces. After mapping the histological section in the tomography volume, we registered the histology sections and tomography slices in 2D, using the Demon registration tool[19] with affine transformation constraints to account for deformations induced by histological sectioning. For the registration, the four histological sections were grey-scaled. The tomography data was colour inverted in order to have a positive correlation to the histological data.

3. RESULTS AND DISCUSSION

3.1 Registration of tomography data and light microscopy-based imaging of histological sections

Figure 3 presents results of the 2D-3D registration of grey-scaled histological section (Fig. 3A) to the tomography data based on polynomials with varying model type fitting. From the qualitative perspective all registered tomography slices look comparable to the histological section.

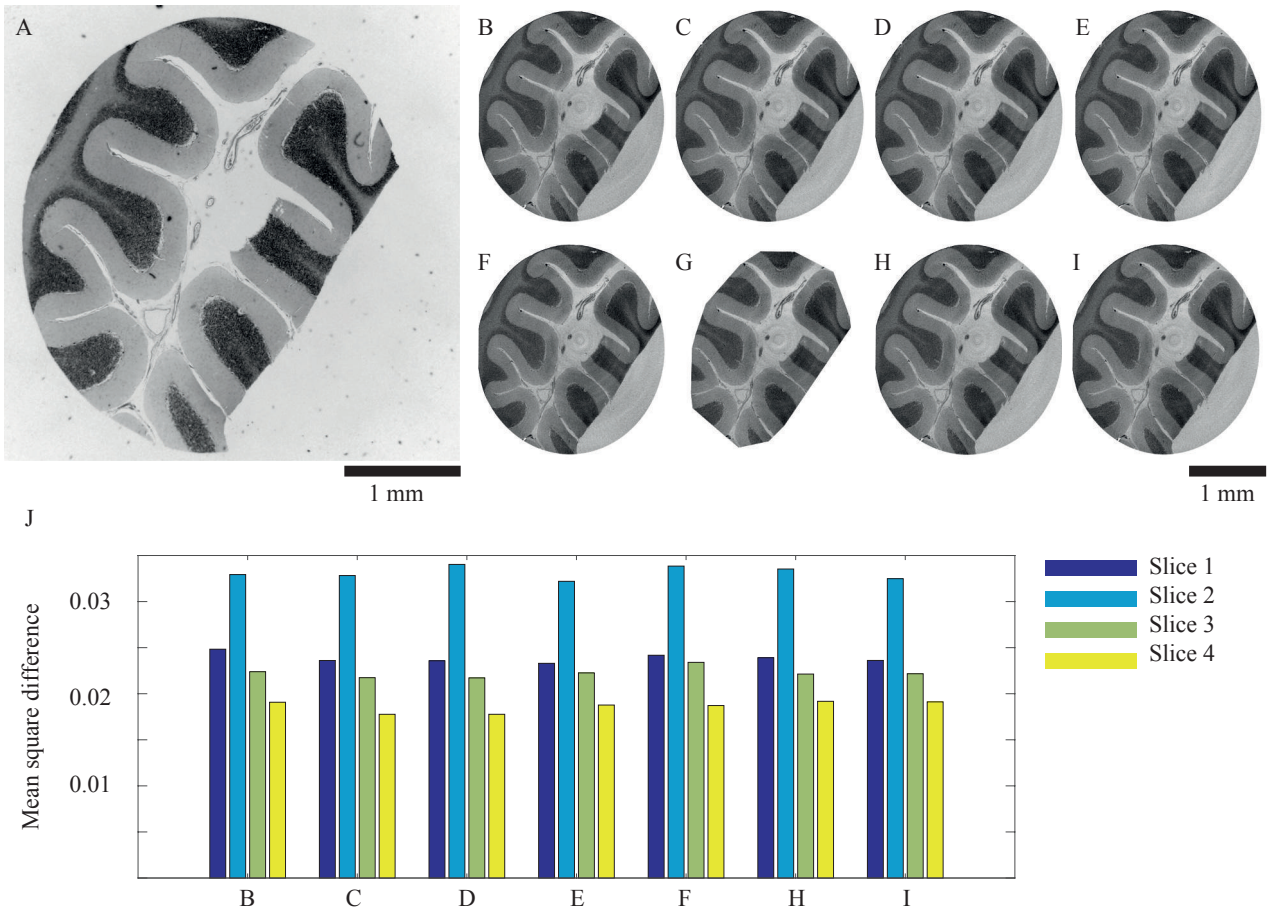

Figure 3. 2D-3D registration of histological section (A) to the tomography data based on polynomial with varying model type fitting to the manually selected landmarks: (B) quadratic polynomial surface, (C) polynomial surface with degree two in one axis and three in other, (D) cubic polynomial surface, (E) polynomial surface with degree four, (F) polynomial surface with degree five, (G) polynomial surface based on piecewise cubic interpolation of landmarks, (H) polynomial surface based on local linear regression of landmarks, (I) polynomial surface based on thin plate model. J: histogram of mean square difference (MSD) between four histological sections and registered to them tomography slices based on selected fitting models.

For the quantitative comparison of selected fitting models, the mean square difference (MSD) between four histological sections and the corresponding tomography slices was calculated, see Figure 3J. MSD is a common

similarity measure that denotes the sum of squared differences between normalised intensity pairs.[20] It can be seen that all fitting models provide comparable results within an equivalent times. The highest deviation between tomography slice and histological section is for histological section 2 and the lowest for histological section 4.

Figure 4 presents the four histological sections (Fig. 4A - D) that were grey-scaled (Fig. 4E - H) and registered to the tomography volume based on ″poly22″ tomography slices are shown in Figure 4I - L. The polynomial surface fit provides reasonable correlation in regions of high landmark density;[13] but, also significantly diverges outside these regions. Regions presenting a limited number of landmarks are comparatively small, nevertheless these regions are not homogeneously distributed and are predominant in some histological sections. These differences, however, are not pronounced, and the visual quality of the registration is preserved for all slices.

Manual 2D-3D registration of a single histological section to the µCT volume is a time-consuming process.[21] Thus, the expert-based registration should be performed mainly for the validation of an automatic approach,[22] as at the current stage registration results of semi-automatic approach are superior then of the automatic one.

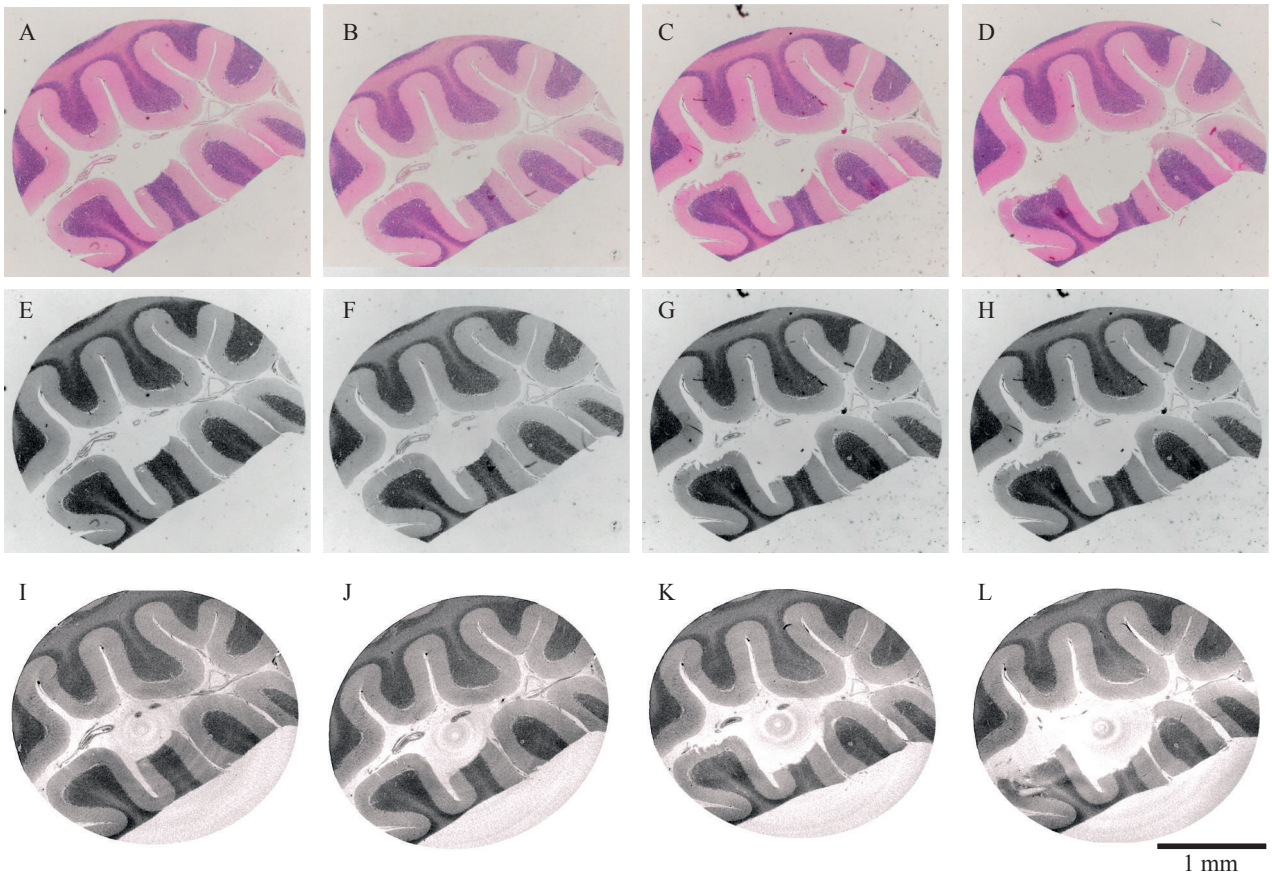

Figure 4. Four histological sections (A - D) were grey-scaled (E - H) and registered to the tomography data set. I - J: Registered tomography slices (poly23).

3.2 Comparison of tomography data and light microscopy-based imaging of histological sections

Figure 5 displays zoomins of the registered human cerebellum slices (E - H) and histological sections (A - D). Both µCT and histology clearly differentiate blood vessels, *Stratum moleculare*, *Stratum granulosum*, white matter, and individual Purkinje cells. In both modalities similar amount of anatomical features can be discriminated.

Fig. 5I shows an image of the selected tomography volume converted into RGB colour space. Colour inverted tomographic slices were transformed into a RGB colour space of histology based on quadratic interpolation,

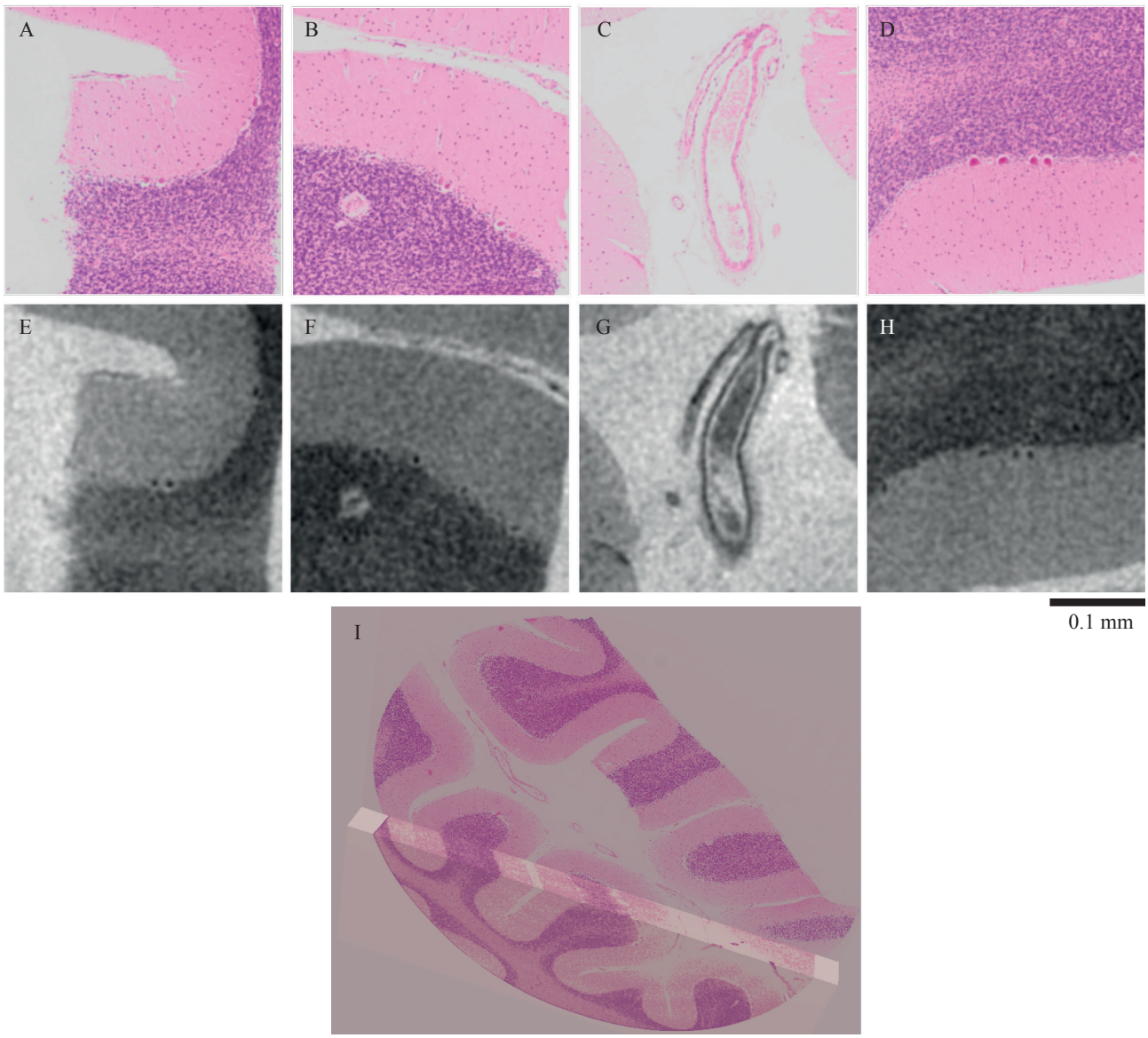

Figure 5. Virtual histology by colourised µCT. A - D: magnifications into histological sections. E - H: registered tomography slices. I: registered tomography volume converted into an RGB colour space to resemble the H&E-stained histological sections (A - D).

respectively, through component-wise histogram equalisation.[13] Pseudo-coloured µCT enhances the display of the images for medical review purposes, for example.

4. CONCLUSION AND OUTLOOK

Histological examination reaches sub-micrometer resolution laterally and enables application of a variety of biochemical tests to the tissue, such as histochemical stains, antibodies, *in situ* nucleic acids hybridization etc. In the third dimension, however, the resolution is limited to the slice thickness. In addition, histological processing introduces tissue-dependent stress and strain into slices which create more or less severe defects.

In contrast, state-of-the-art hard X-ray micro computed tomography (µCT) systems provide isotropic submicrometer resolution, avoid sectioning artefacts and do not require staining. In this communication, we demon-

strated that paraffin-embedded human cerebellum yields appropriate absorption-contrast in laboratory-based µCT data, which is comparable to staining intensity of conventional histological sections.

At the current stage, the spatial resolution and contrast of histological data is superior to that of µCT. Nevertheless, correction of histological data by less detailed tomography can be performed.[24] Registration of histological sections into the tomography volume enables extension of histology into the third dimension, extrapolating findings from histochemistry of a single section over a complete tissue volume. The results indicate that laboratory-based µCT is the modality to fill the current performance gap between synchrotron radiation-based µCT and histological examination for a variety of soft tissue specimens.

5. ACKNOWLEDGEMENTS

The authors acknowledge the financial support of the Swiss National Science Foundation (SNSF) projects 147172, 150164 and SNSF R'Equip project 133802. The authors are thankful to all members of the BMC team for their helpful discussions.

REFERENCES

[1] Dasgupta, A., Das, R., Nayak, L., and De, R., "Analyzing epileptogenic brain connectivity networks using clinical EEG data," *Proc. IEEE BIBM* (7359791), 815–821 (2015).

[2] Power, J. D., Cohen, A. L., Nelson, S. M., Wig, G. S., Barnes, K. A., Church, J. A., Vogel, A. C., Laumann, T. O., Miezin, F. M., Schlaggar, B. L., and Petersen, S. E., "Functional network organization of the human brain," *Neuron* **72**(4), 665 – 678 (2011).

[3] Krauth, A., Blanc, R., Poveda, A., Jeanmonod, D., Morel, A., and Székely, G., "A mean three-dimensional atlas of the human thalamus: Generation from multiple histological data," *NeuroImage* **49**(3), 2053–2062 (2010).

[4] Richardson, D. S. and Lichtman, J. W., "Clarifying tissue clearing," *Cell* **162**(2), 246–257 (2015).

[5] Oh, S. W., Harris, J. A., Ng, L., Winslow, B., Cain, N., Mihalas, S., Wang, Q., Lau, C., Kuan, L., Henry, A. M., Mortrud, M. T., Ouellette, B., Nguyen, T. N., Sorensen, S. A., Slaughterbeck, C. R., Wakeman, W., Li, Y., Feng, D., Ho, A., Nicholas, E., Hirokawa, K. E., Bohn, P., Joines, K. M., Peng, H., Hawrylycz, M. J., Phillips, J. W., Hohmann, J. G., Wohnoutka, P., Gerfen, C. R., Koch, C., Bernard, A., Dang, C., Jones, A. R., and Zeng, H., "A mesoscale connectome of the mouse brain," *Nature* **508**(7495), 207–214 (2014).

[6] Helmstaedter, M., "Cellular-resolution connectomics: Challenges of dense neural circuit reconstruction," *Nat. Methods* **10**(6), 501–507 (2013).

[7] Silvestri, L., Costantini, I., Sacconi, L., and Pavone, F., "Clearing of fixed tissue: A review from a microscopist's perspective," *J. Biomed. Optics* **21**(8), 081205 (2016).

[8] Chung, K., Wallace, J., Kim, S.-Y., Kalyanasundaram, S., Andalman, A. S., Davidson, T. J., Mirzabekov, J. J., Zalocusky, K. A., Mattis, J., Denisin, A. K., Pak, S., Bernstein, H., Ramakrishnan, C., Grosenick, L., Gradinaru, V., and Deisseroth, K., "Structural and molecular interrogation of intact biological systems," *Nature* **497**(7449), 332–337 (2013).

[9] Murray, E., Cho, J. H., Goodwin, D., Ku, T., Swaney, J., Kim, S.-Y., Choi, H., Park, Y.-G., Park, J.-Y., Hubbert, A., McCue, M., Vassallo, S., Bakh, N., Frosch, M. P., Wedeen, V. J., Seung, H. S., and Chung, K., "Simple, scalable proteomic imaging for high-dimensional profiling of intact systems," *Cell* **163**(6), 1500–1514 (2015).

[10] Lareida, A., Beckmann, F., Schrott-Fischer, A., Glueckert, R., Freysinger, W., and Müller, B., "High-resolution x-ray tomography of the human inner ear: Synchrotron radiation-based study of nerve fibre bundles, membranes and ganglion cells," *J. Microsc.* **234**(1), 95–102 (2009).

[11] Schulz, G., Weitkamp, T., Zanette, I., Pfeiffer, F., Beckmann, F., David, C., Rutishauser, S., Reznikova, E., and Müller, B., "High-resolution tomographic imaging of a human cerebellum: Comparison of absorption and grating-based phase contrast," *J. R. Soc. Interface* **7**(53), 1665–1676 (2010).

[12] Hieber, S. E., Bikis, C., Khimchenko, A., Schweighauser, G., Hench, J., Chicherova, N., Schulz, G., and Müller, B., "Tomographic brain imaging with nucleolar detail and automatic cell counting," *Sci. Rep.* **6**, 32156 (2016).

[13] Khimchenko, A., Deyhle, H., Schulz, G., Schweighauser, G., Hench, J., Chicherova, N., Bikis, C., Hieber, S., and Müller, B., "Extending two-dimensional histology into the third dimension through conventional micro computed tomography," *NeuroImage* **139**, 26–36 (2016).

[14] Wenz, J., Schleede, S., Khrennikov, K., Bech, M., Thibault, P., Heigoldt, M., Pfeiffer, F., and Karsch, S., "Quantitative X-ray phase-contrast microtomography from a compact laser-driven betatron source," *Nat. Commun.* **6**, 7568 (2015).

[15] General Electric, Measurement and Control, "Phoenix nanotom m 180 kV / 20 W X-ray nanoCT system for high-resolution analysis and 3D metrology, https://www.gemeasurement.com/inspection-ndt/radiography-and-computed-tomography/phoenix-nanotom-m," (26.09.2016).

[16] Egbert, A. and Brunke, O., "High-resolution X-ray computed tomography for materials research," *Adv. Mat. Res.* **222**, 48–51 (2011).

[17] Museyko, O., Marshall, R., Lu, J., Hess, A., Schett, G., Amling, M., Kalender, W., and Engelke, K., "Registration of 2D histological sections with 3D micro-CT datasets from small animal vertebrae and tibiae," *Comput. Methods Biomech. Biomed. Eng.* **18**(15), 1658–1673 (2015).

[18] Markelj, P., Tomaževič, D., Likar, B., and Pernuš, F., "A review of 3D/2D registration methods for image-guided interventions," *Med. Image Anal.* **16**(3), 642–661 (2012).

[19] Kroon, D.-J. and Slump, C., "MRI modalitiy transformation in demon registration," *Proc. ISBI: From Nano to Macro* **1**(5193214), 963–966 (2009).

[20] Razlighi, Q., Kehtarnavaz, N., and Yousefi, S., "Evaluating similarity measures for brain image registration," *J. Vis. Commun. Image Represent.* **24**(7), 977–987 (2013).

[21] Hoerth, R., Baum, D., Kntel, D., Prohaska, S., Willie, B., Duda, G., Hege, H.-C., Fratzl, P., and Wagermaier, W., "Registering 2D and 3D imaging data of bone during healing," *Connect. Tissue Res.* **56**(2), 133–143 (2015).

[22] Chicherova, N., Hieber, S., Schulz, G., Khimchenko, A., Bikis, C., Cattin, P., and Müller, B., "Automatic histology registration in application to X-ray modalities," *Proc. SPIE* **9967**, 996708 (2016).

[23] Hewitt, S., Lewis, F., Cao, Y., Conrad, R., Cronin, M., Danenberg, K., Goralski, T., Langmore, J., Raja, R., Williams, P., Palma, J., and Warrington, J., "Tissue handling and specimen preparation in surgical pathology: Issues concerning the recovery of nucleic acids from formalin-fixed, paraffin-embedded tissue," *Arch. Pathol. Lab. Med.* **132**(12), 1929–1935 (2008).

[24] Germann, M., Morel, A., Beckmann, F., Andronache, A., Jeanmonod, D., and Müller, B., "Strain fields in histological slices of brain tissue determined by synchrotron radiation-based micro computed tomography," *J. Neurosci. Meth.* **170**(1), 149–155 (2008).